Prediction of Sorption of CO_2 in Glassy Atactic Polystyrene at Elevated Pressures Through a New Computational Scheme

Theodora Spyriouni,[†,‡] Georgios C. Boulougouris,[‡,§] and Doros N. Theodorou*[,†,§]

Institute of Physical Chemistry, NCSR "Demokritos", Aghia Paraskevi Attikis, 153 10 Athens, Greece, Scienomics SARL, 17, Square Eduard VII, 75009 Paris, France, and Department of Materials Science and Engineering, School of Chemical Engineering, National Technical University of Athens, 9 Heroon Polytechniou, Zografou Campus, Athens 15780, Greece

Received July 8, 2008; Revised Manuscript Received November 14, 2008

ABSTRACT: A strategy allowing the computation of sorption isotherms, up to high penetrant activities, in glassy matrices has been designed. The new scheme permits an equilibrium repartition of the solute molecules in the matrix. The scheme is coupled to an efficient methodology for the calculation of the penetrant fugacity, namely, the direct particle deletion method, a generalization of the staged particle deletion method. The sorption isotherms of CO_2 in atactic polystyrene (PS) and the induced polymer swelling have been calculated in the temperature range from 308 to 405 K for pressures up to 300 bar. The results compare favorably to available experimental data. Larger deviations are observed at low temperatures and high pressures, most probably due to the long relaxation times of the polymer matrix. Derivative properties, such as the partial molar volume and the partial molar enthalpy of CO_2, have been calculated in good agreement with experimental findings. The segmental dynamics of PS have been analyzed, and the pressure-induced glass transition (P_g) has been calculated for various temperatures below the T_g of pure PS. The results compare well with experimental data. The analysis of the free volume of the polymer matrix in the CO_2/PS systems showed higher free volumes at higher temperatures because of polymer swelling.

Introduction

The sorption of some gases in amorphous polymers plastifies the polymers, that is, causes a reduction in the glass-transition temperature (sorption-induced glass transition (SIGT) phenomenon), which seriously affects the thermophysical and mechanical properties of the polymer. Supercritical CO_2 is widely used as a plasticizer because its critical properties (304 K and 73 bar) permit operation under mild conditions. Atactic polystyrene (PS), which is glassy under ambient conditions, is one of the most widely used polymers. Numerous studies, both experimental and theoretical, on the solubility of CO_2 in PS have appeared in the literature within the last two decades. A very recent investigation is that of Panayiotou and collaborators,[1] who measured the sorption of CO_2 in PS by using two experimental techniques, that is, the quartz crystal microbalance and the mass-loss analysis, over a wide spectrum of temperatures and up to very high pressures. In a subsequent paper,[2] they also reported swelling of glassy matrices (poly(methyl methacrylate) (PMMA) and PS) due to CO_2 sorption, which was measured by means of a magnetic suspension balance method. In both papers, they compare their results with a recently developed equation of state based on the nonrandom hydrogen bonding (NRHB) model.[3] Wissinger and Paulaitis[4] measured CO_2 sorption and polymer swelling of polycarbonate (PC), PMMA, and PS at 33−65 °C and pressures up to 100 atm by means of a quartz spring balance. They, too, developed a thermodynamic approach for predicting sorption and swelling in glassy polymer−solute systems on the basis of a lattice model for polymer solutions and the concept of order parameters to describe the glassy state.[5] Conforti et al.[6] used the pressure decay method to measure sorption in PS at 35 °C and at low pressures below 40 bar. Aubert[7] used the quartz crystal microbalance method to measure CO_2 solubility in PS at 40 °C and pressures up to 100 bar. Zhang et al.[8] measured CO_2 sorption and swelling in PS, PMMA, and other polymers and block copolymers at 35 °C and pressures up to 100 bar by using a quartz spring technique and a cathetometer. Sato et al.[9] measured sorption of CO_2 in molten PS at 373.2 and 453.2 K and pressures up to 200 bar by using a pressure decaying method. Hilic et al.[10] used a combined technique of a pressure decay apparatus with a vibrating-wire force sensor to measure sorption and swelling in PS at 338 to 402 K for pressures up to 450 bar. Chang et al.[11] used a gravimetric sorption method similar to that in ref 4 and a cathetometer to measure sorption and swelling in glassy and rubbery polymers. They observed a sigmoidal increase in sorption with pressure for the rubbers and an increase/leveling-off for the glassy polymers. Shieh and Liu[12] studied sorption and CO_2/PS interactions by using mass-loss analysis and FTIR spectroscopy at 32 °C and pressures up to 350 bar. Vogt et al.[13] studied the effect of CO_2 sorption on the phase behavior of two PS copolymers by the pressure decay method at 60 and 100 °C and pressures up to 120 bar. Toi and Paul[14] studied the effect of the PS molecular weight on sorption isotherm of CO_2 at 35−55 °C and up to 25 atm. For the determination of the SIGT point, several studies have appeared that are based on inverse supercritical chromatography and differential scanning calorimetry.[1,5,15,16]

On the theoretical/simulation front, an innovative study of sorption, swelling, and plasticization phenomena in glassy polymers was conducted by Van der Vegt et al.,[17] who calculated sorption isotherms of CO_2 in a hypothetical glassy polymer of $T_g \cong 500$ K. In their earlier work, Gusev and Suter[18] calculated sorption isotherms as averages over a large number of independent polymer/solute configurations. Cuthbert et al.[19] calculated the excess chemical potential of gases in a PS glass generated on a lattice by means of the Widom insertion method and a modified excluded volume map sampling algorithm. Fukuda[20] calculated solubility coefficients of several gases in amorphous polyethylene with excluded volume map sampling.[21]

The great importance of plasticization phenomena caused by supercritical fluids in glassy polymers and the abundance of

* Corresponding author. E-mail: doros@central.ntua.gr.
† NCSR "Demokritos".
‡ Scienomics SARL.
§ National Technical University of Athens.

10.1021/ma8015294 CCC: $40.75
Published on Web 02/05/2009

experimental data for the specific system CO_2/PS motivated our interest in studying this system by molecular simulation. Unlike most previous studies, we aimed at modeling sorption, swelling, and plasticization in atomistic detail, permitting a direct comparison with experiments. Although significant advances have been made in our ability to sample the long-time dynamics in glasses,[22] once they are formed, the main challenges presented by this type of study are (a) the generation of realistic configurations of the glassy polymer, (b) the sufficient sampling of the solute distribution in the polymer matrix given the solute's limited diffusivity, and (c) the calculation of the solute chemical potential given that the penetrant is too large for the traditional Widom insertion method to be efficiently performed.

In this work, we have addressed each of the above challenges by (a) generating realistic configurations of glassy PS through a recently developed coarse-graining and reverse mapping scheme,[23] (b) introducing a new strategy that permits fast equilibrium repartitioning of the solute in the polymer matrix in the course of a molecular dynamics (MD) simulation, and (c) using the direct particle deletion (DPD) method,[24] an extension of the staged particle deletion (SPD) method, for the efficient calculation of sorbate chemical potentials.[24−26]

Methodology. *Molecular Model and Simulation Conditions.*

The atomistic configurations of PS were obtained according to the coarse-graining equilibration reverse-mapping strategy described in ref 23. As described in ref 23, at the coarse-grained level, each diad along the PS chain was represented as a single interaction site, or superatom. In the same reference, a new method was proposed for reverse-mapping the equilibrated coarse-grained melt configurations to a detailed united-atom model of PS without charges, which consisted of aliphatic CH_2, CH, and CH_3 and aromatic CH centers. A detailed description of the united-atom model is given in Table 1. CO_2 was represented as a rigid triatomic linear molecule according to the Harris and Yung model.[27] The polymer matrix of the simulated systems consisted of 3 chains of monodisperse atactic PS with 150 monomers each (3627 sites in total). To check for system size effects, a bigger polymer matrix consisting of 4 chains with 200 monomers each (6436 sites in total) was also simulated at the lower temperature.

The initial configuration of the pure polymer was an equilibrated reverse-mapped melt configuration at $T = 413$ K and $P = 1$ bar that was obtained using the strategy described in ref 23. Chain conformations in model PS melts obtained through this strategy were found to be equilibrated on all length scales. Chain dimensions, as predicted from the mean-square end-to-end distance and its distribution, from the mean-square radius of gyration, from the characteristic ratio, and from the single chain scattering function (Kratky plot) were found to be in excellent agreement with available experimental evidence.[23] The predicted mass density in the melt was very close to the experimental value. The X-ray diffraction pattern computed from reverse-mapped melt configurations[23] was in favorable agreement with experimental patterns from molten atactic PS. Furthermore, extensive local equilibration following reverse mapping improved the torsion angle distributions for meso- and racemic diads relative to the results presented in ref 23, bringing them very close to theoretical expectations for the model employed and to experimental estimates from NMR spectroscopy.

Reverse-mapped melt configurations of a PS were cooled isobarically at a rate of −6 K/ns to $T = 308$ K with a series of isothermal−isobaric (NPT) MD simulations by the use of the large-scale atomic/molecular massively parallel simulator program (LAMMPS[28]). A glassy PS configuration was thus generated for each system size. Five isotherms were generated at $T = 35$, 50, 81, 100, and 132 °C for pressures up to 300 bar.

Table 1. United-Atom Force Field for PS (Chain Structure: $CH_3-CH-(C_6H_5)-[CH_2-CH-(C_6H_5)-]_{n_u}-CH_3$)

1. Nonbonded Interactions

$U_{nb} = \varepsilon[(r_0/r)^{12} - 2(r_0/r)^6]$; $\varepsilon = (\varepsilon_1\varepsilon_2)^{0.5}$, $r_0 = (r_{0,1} + r_{0,2})/2$

$\varepsilon = 0.12$ kcal·mol^{-1}, $r_0 = 4.321$ Å for CH_2

$\varepsilon = 0.09$ kcal·mol^{-1}, $r_0 = 4.153$ Å for aliphatic CH

$\varepsilon = 0.12$ kcal·mol^{-1}, $r_0 = 4.153$ Å for aromatic C and CH

cutoff distance = 9 Å. Interactions taken between sites separated by three or more bonds. No nonbonded interactions considered within phenyl rings.

2. Bond Lengths

$U_l = k_l(l - l_0)^2$

$k_l = 317$ kcal·mol^{-1}·Å^{-2}, $l_0 = 1.53$ Å for aliphatic CH_2-CH

$k_l = 317$ kcal·mol^{-1}·Å^{-2}, $l_0 = 1.51$ Å for CH(aliph)−C(arom)

$k_l = 525$ kcal·mol^{-1}·Å^{-2}, $l_0 = 1.40$ Å for CH(arom)−CH(arom)

3. Bond Angles

$U_\theta = k_\theta(\theta - \theta_0)^2$

$k_\theta = 60$ kcal·mol^{-1}·rad^{-2}, $\theta_0 = 109.5°$ for aliphatic $CH_2-CH-CH_2$

$k_\theta = 63$ kcal·mol^{-1}·rad^{-2}, $\theta_0 = 109.5°$ for aliphatic $CH-CH_2-CH$

$k_\theta = 60$ kcal·mol^{-1}·rad^{-2}, $\theta_0 = 109.5°$ for CH_2(aliph)−CH(aliph)−C(arom)

$k_\theta = 70$ kcal·mol^{-1}·rad^{-2}, $\theta_0 = 120°$ for CH(aliph)−C(arom)−CH(arom)

$k_\theta = 72$ kcal·mol^{-1}·rad^{-2}, $\theta_0 = 120°$ for CH(arom)−CH(arom)−CH(arom)

4. Backbone Torsion (X−CH(aliph)−CH_2(aliph)−X)

$U_\varphi = k_\varphi(1 - \cos 3\varphi)$

$k_\varphi = 1.4$ kcal·mol^{-1}

(trans taken as $\varphi = 0$)

5. Torsion CH_2(aliph)−CH_2(aliph)−CH(arom)−CH(arom)

(phenyl ring torsion around CH(aliph)−C(arom))

$U_\varphi = k_\varphi\ (1 + \cos 2\varphi)$

$k_\varphi = 1$ kcal·mol^{-1}

(phenyl parallel to backbone taken as $\varphi = 0$)

6. Torsion CH(arom)−CH(arom)−CH(arom)−CH(arom)

$U_\varphi = k_\varphi(1 - \cos 2\varphi)$

$k_\varphi = 12.9$ kcal·mol^{-1}

(planar configuration taken as $\varphi = 0$)

7. Improper Torsion (C(arom)−CH(aliph)−CH_2(aliph)−CH_2(aliph))

(to maintain chirality)

$U^{chir}(f_{chir}) = \kappa/(1-f_{chir}) - [\kappa f^2_{chir}/(1-\delta)^3] + [\kappa(3\delta-1)f_{chir}/(1-\delta)^2] - [\kappa(3\delta^2 - 3\delta + 1)/(1-\delta)^3]$

$f_{chir} = [(\cos^2\alpha + \cos^2\beta + 2\cos\alpha\cos\beta\cos\theta)/\sin^2\theta] \le 1$

$\kappa = 0.05$ kcal·mol^{-1}, $\delta = 0.4$

bond angles:

π-α: CH_2(aliph)−CH(aliph)−C(arom), π-β: C(arom)−CH(aliph)−CH_2(aliph)

π-θ: CH_2(aliph)−CH(aliph)−CH_2(aliph)

The large temperature and pressure range investigated extends from the glassy state to the plastified polymer and the melt. The pure polymer matrix was initially equilibrated at each temperature via an NPT MD run of 20 ns duration and was then progressively loaded with increasing amounts of CO_2. Equations of motion were integrated in Cartesian coordinates. CO_2 molecules were treated as rigid bodies, and their positions and velocities were updated with constant-energy time integration. CO_2 molecules thermalized via their interactions with the polymer matrix. A switching function (spline fit) of LAMMPS was applied to the short-range nonbonded potential within a switching region (from 6.7 to 7.3 Å) so that energy and force would go smoothly to zero. Long-range electrostatic interactions between CO_2 molecules were treated with a group-based cutoff and were set to 15 Å in this work so that interactions between two molecules were taken into account either fully or not at all.

Scheme for Repartitioning Penetrant Molecules among Cavities. We loaded glassy matrices of PS obtained as described above with CO_2 at various compositions by mapping the accessible free volume.[29] The loaded matrices were subjected to MD simulations at constant temperature, pressure, and number of molecules of each component (N_1N_2PT ensemble).

In the course of each N_1N_2PT simulation, the solute was redistributed among the accessible cavities to achieve an

equilibrium repartitioning within the thermally fluctuating polymer matrix. This was accomplished by periodically selecting (every 5 to 6 ps) one configuration and attempting a certain number of CO_2 displacements between the accessible cavities (~2000 attempts per CO_2 molecule; see graphical depiction in Supporting Information). More specifically, the polymer matrix (without the solute molecules) was subjected to geometric analysis, that is, Delaunay tessellation, followed by volume and connectivity analysis as implemented by Greenfield and Theodorou[29] and Dodd and Theodorou[30] to determine the clusters of sites where a spherical solute of specific radius can reside. To keep the algorithm simple and fast, we looked for cavities accessible to a spherical particle with a radius equal to the LJ radius of the C atom of CO_2. Thus, not all cavities were able to accommodate a CO_2 molecule, but small cavities in which a CO_2 could fit with a specific orientation would not be missed. In the course of a CO_2 displacement between cavities, one CO_2 molecule, residing in a cavity (old) consisting of *NT*cav Delaunay tetrahedra, was selected at random. The tetrahedron containing the center of the CO_2 molecule was identified, and its volume (*VT*cav) was recorded. Subsequently, a destination cavity (new) was randomly selected, and from that cavity one tetrahedron was picked up at random. The CO_2 molecule was removed from its old position and placed at a random orientation with its center at a random position within the selected tetrahedron. The Boltzmann factor of the associated energy change, ΔU, was calculated. The exchange move was accepted according to the probability

$$p = \frac{VT\text{cav}_{\text{new}} NT\text{cav}_{\text{new}}}{VT\text{cav}_{\text{old}} NT\text{cav}_{\text{old}}} \exp(-\beta \Delta U) \quad (1)$$

with $\beta = 1/(k_B T)$, where k_B is the Boltzmann constant. Following the acceptance or rejection of the attempted repartitioning moves, we proceeded with the molecular dynamics simulation of the polymer−solute system with all particle velocities reinitialized.

A computer animation displaying the identification of accessible cavities within the CO_2−PS system and the scheme for repartitioning CO_2 molecules among these cavities is available in the Supporting Informationaccompanying this article.

Iterative Scheme for Equilibration with a Pure Gas Phase. Our intention in these N_1N_2PT simulations was to sample a polymer phase at equilibrium with a pure CO_2 gas phase at the prevailing pressure P and temperature T. The excess chemical potential of CO_2, μ_2^{ex}, was calculated using the DPD method,[24] a generalization of SPD[25] (please see below). The fugacity of CO_2 in the polymer matrix was calculated from the excess chemical potential via the relationship

$$f_{CO_2} = f_2 = N_2 k_B T \left\langle \frac{1}{V} \right\rangle \exp(\beta \mu_2^{ex}) \quad (2)$$

where N_2 is the number of CO_2 molecules in the polymer matrix and $\langle 1/V \rangle$ is the average inverse volume under N_1N_2PT conditions. We calculated a new pressure, P, via the SAFT equation of state[31] for pure gaseous CO_2 by setting the gas-phase fugacity equal to f_{CO_2}. The N_1N_2PT MD simulation was continued for ca. 14 ns at the new pressure, and the pressure was revised again, if necessary, until the CO_2 fugacity in the polymer matrix and in the gas were equal. This iterative scheme converged rapidly because the CO_2 fugacity in the polymer was not very sensitive to the pressure. At the converged value of P, the last 7 ns of the run (half of the run) was the production phase of the N_1N_2PT MD simulation. Throughout the production phase, the volume and CO_2 chemical potential fluctuated around constant values.

Chemical Potential Calculation with the Direct Particle Deletion Method. One of the first, and probably the simplest and most widely used, methods for evaluating chemical potential in molecular simulations is the Widom insertion method.[32] Widom's method gave us the ability to combine the stochastic integration that creates the Markovian chain of microstates for the calculation of ensemble averages with a second integration over the degrees of freedom of an additional ghost particle for the first time. In this way, it allowed the evaluation of the ratio of the partition functions of the perturbed ($N + 1$ molecules) and the reference (N molecules) systems. Recently, Boulougouris and Frenkel showed[33] that it is possible to combine several levels of integration (stochastic or not) on the basis of the integration over a Markovian web (IMW) formalism in the evaluation of any given observable, not just the chemical potential. IMW, like Widom insertion, allows the use of ghost moves (not only insertions but also any valid Monte Carlo move) and enriches the ensemble average by including the result of all possible outcomes of real and ghost moves. Unfortunately, as the system becomes denser and the solute molecules become bigger, the traditional Widom insertion method for the calculation of solubilities[32] is of limited use; similar difficulties arise in the case in which solute molecules exhibit strong, specific interactions with the matrix. To facilitate insertions, several techniques have appeared, such as (a) the configurational-bias method,[34] which grows the solute molecule in a bond-by-bond fashion; (b) the free energy perturbation, where a coupling parameter modulates the solute−matrix interactions and the solubility is obtained by thermodynamic integration (TI) over a number of simulations conducted at different values of the coupling parameter;[35] (c) the expanded ensemble scheme, which permits calculation of free energy differences between thermodynamic states and can be thought of as an application of the free energy perturbation method but within a single simulation;[36] (d) the extended ensemble MD method, where the coupling of the solute with the rest of the system is continuously changing, allowing the solute to escape from low-energy pockets and explore all of the accessible volume;[37] and (e) the minimum mapping (minmap) method,[38] which brings about local configurational changes in the vicinity of the inserted molecule to alleviate unfavorable (e.g., excluded volume) interactions. Another approach, the fast growth TI method,[39] based on Jarzynski's nonequilibrium work theorem,[40] allows the calculation of the chemical potential via several independent TI runs.

In this section, we provide the formal derivation of the DPD method for the first time. DPD was developed several years ago in the context of the Ph.D. thesis of G. C. Boulougouris.[24] Although it has been successfully applied since then,[41] the formal derivation appears only in the thesis. The final expression of DPD can be considered to be a generalization of the SPD.[25] In reality, however, the method is based on the introduction of a completely different thermodynamic perturbation scheme. One can always envision the deletion or insertion of a molecule to be a transformation of a real molecule to an ideal gas molecule and vice versa. Both SPD and the initial Widom insertion method are based on a configuration by configuration comparison; that is, in a configuration of the reference system, a perturbation is performed by deleting or randomly inserting a molecule. The important aspect in this process is that because this is a first-order perturbation the molecules in the configuration are not allowed to relax from the state sampled by the reference system. There is a big difference, however, between adding and removing molecules. In the case of inserting molecules, both perturbed and reference systems sample the same configuration space. That is, both ideal and ghost inserted molecules are allowed to visit all of the positions in the box. In the case of the molecule removal, however, the removed molecule is not allowed to access all positions in the simulation box because it is bounded by the presence of the $N - 1$ remaining molecules; it is allowed to access only a small part

of that volume, that is, the volume accessible to it. Whereas SPD introduces an intermediate state, that of $N-1$ molecules and one cavity to overcome this bias, DPD proposes a novel and more drastic approach in which the perturbation is performed over all possible positions of the removed molecules and is integrated over all of these positions.

The mathematical formulation presented here concerns simulation in the N_1N_2PT ensemble. The Gibbs energy of a system of N_1 solvent molecules and N_2 solute molecules at temperature T and pressure P can be calculated from the expression

$$G(N_1,N_2,P,T) = -\frac{1}{\beta}\ln(Q(N_1,N_2,P,T)) \tag{3}$$

where $Q(N_1,N_2,P,T)$ is the isothermal−isobaric partition function of the system and $\beta \equiv 1/(k_BT)$. Subsequently, the chemical potential of the solute is calculated from the expression

$$\begin{aligned}\beta\mu_2 &= \beta\left.\frac{\partial G}{\partial N_2}\right|_{N_1,P,T} \\ &= \beta\frac{G(N_1,N_2,P,T)-G(N_1,N_2-1,P,T)}{N_2-(N_2-1)} \\ &= -\ln\frac{Q(N_1,N_2,P,T)}{Q(N_1,N_2-1,P,T)} \\ &= -\ln\left(\frac{(N_2-1)!\,\Lambda_2^{3(N_2-1)m}}{N_2!\,\Lambda_2^{3N_2m}}\frac{Z(N_1,N_2,P,T)}{Z(N_1,N_2-1,P,T)}\right)\end{aligned} \tag{4}$$

where m is the number of sites (atoms) constituting a solute molecule (these sites assumed here to be of equal mass without loss of generality), Λ_2 is the thermal wavelength of such an atom, and $Z(N_1,N_2,P,T)$ stands for the configurational integral in the N_1N_2PT ensemble, including all intra- and intermolecular contributions to the potential energy. Equation 4 gives the total chemical potential, whereas for most applications, it is the excess chemical potential that is more practical to use. The ideal gas chemical potential of the pure solute at temperature T and molecular density $\langle N_2/V\rangle$ is given as $\beta\mu_2^{ig} = \ln(\langle N_2/V\rangle(\Lambda_2^{3m}/Z_2^{intra}))$, where $Z_2^{intra} = \int \exp[-\beta U_2^{intra}(\mathbf{q}_{(N_2)})]\,d\mathbf{q}_{(N_2)}$ is the intramolecular configurational integral, $\mathbf{q}_{(N_2)}$ is the vector of internal and orientational degrees of freedom of the N_2^{th} solute molecule, and angular brackets denote averaging in the N_1N_2PT ensemble of our solvent−solute system. If atomic Cartesian coordinates $\mathbf{r}_i^{(N_2)}$ are used to describe the configuration of the N_2^{th} solute molecule, then $\mathbf{q}_{(N_2)}$can be conveniently defined as $\mathbf{q}_{(N_2)} = (\mathbf{r}_2^{(N_2)} - \mathbf{r}_1^{(N_2)}, \mathbf{r}_3^{(N_2)}-\mathbf{r}_2^{(N_2)},..., \mathbf{r}_m^{(N_2)} - \mathbf{r}_{m-1}^{(N_2)})$. It is also convenient to group the degrees of freedom of solute molecules in the system in the following manner: $\mathbf{q}_{N_2-1} \equiv (\mathbf{s}_1^{(1)}, \mathbf{r}_2^{(1)} - \mathbf{r}_1^{(1)},..., \mathbf{r}_m^{(1)} - \mathbf{r}_{m-1}^{(1)},..., \mathbf{s}_1^{(N_2-1)}, \mathbf{r}_2^{(N_2-1)} - \mathbf{r}_1^{(N_2-1)},..., \mathbf{r}_m^{(N_2-1)} - \mathbf{r}_{m-1}^{(N_2-1)})$ is a vector of relative coordinates that characterizes the configuration of solute molecules 1, 2,..., N_2-1. Likewise, $\mathbf{q}_{N_2} \equiv (\mathbf{s}_1^{(1)}, \mathbf{r}_2^{(1)} - \mathbf{r}_1^{(1)},..., \mathbf{r}_m^{(1)} - \mathbf{r}_{m-1}^{(1)},..., \mathbf{s}_1^{(N_2)}, \mathbf{r}_2^{(N_2)} - \mathbf{r}_1^{(N_2)},..., \mathbf{r}_m^{(N_2)} - \mathbf{r}_{m-1}^{(N_2)})$ is a vector of relative coordinates that characterizes the configuration of solute molecules 1, 2,..., N_2. We also introduce $\mathbf{q}_{N_1} \equiv (\mathbf{s}_1^{(1)}, \mathbf{r}_2^{(1)} - \mathbf{r}_1^{(1)},..., \mathbf{r}_l^{(1)} - \mathbf{r}_{l-1}^{(1)},..., \mathbf{s}_1^{(N_1)}, \mathbf{r}_2^{(N_1)} - \mathbf{r}_1^{(N_1)},..., \mathbf{r}_l^{(N_1)} - \mathbf{r}_{l-1}^{(N_1)})$ as the vector that characterizes the configuration of the N_1 solvent molecules in the system with each solvent molecule consisting of l sites. In the case of the N_1N_2PT ensemble considered here, the position vector of the first atom of each molecule (solvent or solute) has been separated and reduced ($\mathbf{s}_1^{(i)} = \mathbf{r}_1^{(i)}/L$) with respect to the current simulation box length (L), giving rise to an integration factor (Jacobian) of V (the box volume) relative to a representation cast in terms of all atomic coordinates. Note that, on the basis of our definitions, $\mathbf{q}_{N_2} \equiv (\mathbf{q}_{N_2-1}, \mathbf{s}_1^{(N_2)}, \mathbf{q}_{(N_2)})$.

We also discern different contributions to the potential energy of the system: $U_2^{intra}(\mathbf{q}_{(N_2)})$ is the intramolecular potential energy of the N_2^{th} single solute molecule, if it is considered to be isolated in configuration $\mathbf{q}_{(N_2)}$. $U(\mathbf{q}_{N_1}, \mathbf{q}_{N_2-1})$ is the total potential energy of the system containing N_2-1 solute molecules and N_1 solvent molecules in the configuration $(\mathbf{q}_{N_1}, \mathbf{q}_{N_2-1})$. Similarly, $U(\mathbf{q}_{N_1}, \mathbf{q}_{N_2})$ is the total potential energy of the system containing N_1 solvent molecules and N_2 solute molecules in the configuration $(\mathbf{q}_{N_1}, \mathbf{q}_{N_2})$. $U_{(N_2)}^{inter}(\mathbf{q}_{N_1}, \mathbf{q}_{N_2})$ is the intermolecular potential energy of interaction between the N_2^{th} solute molecule and the rest of the system (solvent and other solute molecules). By definition

$$U_{(N_2)}^{inter}(\mathbf{q}_{N_1}, \mathbf{q}_{N_2}) = U(\mathbf{q}_{N_1}, \mathbf{q}_{N_2}) - U(\mathbf{q}_{N_1}, \mathbf{q}_{N_2-1}) - U_2^{intra}(\mathbf{q}_{(N_2)}) \tag{5}$$

From eq 4 and the definition of the ideal gas chemical potential, we can express the excess chemical potential as

$$\beta\mu_2^{ex} = \beta\mu_2 - \beta\mu_2^{ig} = -\ln\left(\left\langle\frac{1}{V}\right\rangle\frac{Z(N_1,N_2,P,T)}{Z(N_1,N_2-1,P,T)Z_2^{intra}}\right) \tag{6}$$

Because $Z_2^{intra} = \int \exp[-\beta U_2^{intra}(\mathbf{q}_{(N_2)})]\,d\mathbf{q}_{(N_2)}$ is independent of $\mathbf{q}_{N_2-1}$,$\mathbf{q}_{N_1}$, the ratio of configurational integrals that appears in the logarithm on the right-hand side of eq 6 can be evaluated as

$$\begin{aligned}R_Z &= \frac{Z(N_1,N_2,P,T)}{Z(N_1,N_2-1,P,T)Z_2^{intra}} \\ &= \frac{\int e^{-\beta PV}dV\,Z(N_1,N_2,V,T)}{\int e^{-\beta PV}dV\,Z(N_1,N_2-1,V,T)Z_2^{intra}} \\ &= \frac{\int e^{-\beta PV}V^{N_1+N_2}\,dV\int e^{-\beta U(\mathbf{q}_{N_1},\mathbf{q}_{N_2})}\,d\mathbf{q}_{N_1}\,d\mathbf{q}_{N_2}}{\int e^{-\beta PV}V^{N_1+N_2-1}\,dV\iint e^{-\beta U_2^{intra}(\mathbf{q}_{(N_2)})}\,d\mathbf{q}_{(N_2)}\,e^{-\beta U(\mathbf{q}_{N_1},\mathbf{q}_{N_2-1})}\,d\mathbf{q}_{N_1}\,d\mathbf{q}_{N_2-1}}\end{aligned} \tag{7}$$

Up to this point, we have used the more-or-less standard procedure. The difference in our DPD formulation lies in the next step. We use the following identity to transform the denominator of eq 7

$$\begin{aligned}\int f(y)\,dy &= \int\frac{\int g(x,y)\,dx}{\int g(x,y)\,dx}f(y)\,dy \\ &= \iint\frac{1}{\int g(x,y)\,dx}g(x,y)f(y)\,dx\,dy\end{aligned} \tag{8}$$

Note that eq 8 is true and well behaved for any function $g(x,y)$ for which $\int g(x,y)\,dx$ is not zero when $f(y)$ is not zero. On the contrary, in traditional perturbation schemes (Widom-like and SPD), the derivation is based on a different identity

$$\begin{aligned}\iint f(y)\,dx\,dy &= \iint\frac{g(x,y)}{g(x,y)}f(y)\,dx\,dy \\ &= \iint\frac{1}{g(x,y)}g(x,y)f(y)\,dx\,dy\end{aligned} \tag{9}$$

Although eqs 8 and 9 may look similar at first, they are quite different in physical meaning and, more importantly, in sampling efficiency. The reason can be easily understood if one considers the importance of the functions $f(y)$ and $g(x,y)f(y)$. In traditional perturbation schemes using eq 9, $f(y)$ represents the Boltzmann weight of the energy of one system (e.g., of the reference system in Widom's scheme), whereas $g(x,y)f(y)$ represents the Boltzmann weight of the energy of the other system (e.g., of the

perturbed system). It is well known that the sampling inefficiency of first-order perturbation schemes lies in the fact that $f(y)$and $g(x,y)f(y)$ are nonzero in different parts of the configuration space. This, in turn, translates as a conditional limit of 1 for $g(x,y)/g(x,y)$ for all values where $f(y)$ is nonzero. The difference in the new scheme (DPD) based on eq 8 is that it requires $[\int g(x,y)\,dx]/[\int g(x,y)\,dx]$ to be 1 for all values where $f(y)$ is nonzero; because of the integration present, this is much easier to fulfill. Note that the statistical weights of both the reference and the perturbed system may be considered to have a theoretical positive value in all configuration space; in practice, however, importance sampling in statistical mechanics recognizes that for only a very small part of phase space are the values of these weights significantly different from zero.

One can devise several different particle deletion schemes by playing with the functional form of $\int g(x,y)\,dx$. Here we propose a scheme that utilizes our ability to calculate the accessible volume analytically for any system of fused hard spheres. Another interesting perspective is to perform a reinsertion process, as can trivially be proven by proper selection of the perturbation integral. Our tests on the Lennard-Jones (LJ) fluid have shown that, although reinsertion has better statistics compared with the original Widom insertion scheme, for high densities, the DPD methodology proposed below is more efficient because of its use of the analytical evaluation of accessible volume.

We choose to perturb our system over the accessible volume of the solute molecule under the conditions of fixed internal and orientational degrees of freedom. That is, for the given $\mathbf{q}_{(N_2)}$ defined by the reference configuration ($\mathbf{q}_{N_1}$, $\mathbf{q}_{N_2}$), we evaluate the accessible volume, within configuration ($\mathbf{q}_{N_1}$, $\mathbf{q}_{N_2-1}$), of a "hard solute molecule" in which each atom, i, of the actual N_2^{th} solute molecule is replaced by a hard sphere of diameter d_i in representing its intermolecular interactions with the rest of the system. Note that by keeping the internal and orientational degrees of freedom $\mathbf{q}_{(N_2)}$ fixed, only the three overall translational degrees of freedom of the N_2^{th} solute molecule can be varied. Therefore, the accessible volume that we define as $\int H_{\mathbf{q}_{N_1},\mathbf{q}_{N_2}}(\mathbf{r}_1^{(N_2)},d)\,d\mathbf{r}_1^{(N_2)}$ measures the locus of points where the first atom $\mathbf{r}_1^{(N_2)}$ (or, equivalently, any reference atom) of the N_2^{th} hard solute molecule can be placed such that, given its $\mathbf{q}_{(N_2)}$ vector, there is no overlap between it and the rest of the system. Mathematically, $H_{\mathbf{q}_{N_1},\mathbf{q}_{N_2}}(\mathbf{r}_1^{(N_2)},d)$ is a product of Heaviside functions[25,26] of the distances between atomic centers, i, on the hard solute molecule and atomic centers, j, in the solvent−solute matrix configuration ($\mathbf{q}_{N_1}$,$\mathbf{q}_{N_2-1}$); each Heaviside function switches from 0 to 1 as its argument distance goes through $d_{ij} = (d_i + d_j)/2$. $\int(H_{\mathbf{q}_{N_1},\mathbf{q}_{N_2}}(\mathbf{s}_1^{(N_2)}, d/L)\,d\mathbf{s}_1^{(N_2)} = \int H_{\mathbf{q}_{N_1},\mathbf{q}_{N_2}}(\mathbf{r}_1^{(N_2)}, d)\,d\mathbf{r}_1^{(N_2)}/V$is then, by definition, the accessible volume fraction, that is the volume accessible for insertion of the first atom of the hard solute molecule in orientation and internal configuration $\mathbf{q}_{(N_2)}$ normalized by the total volume of the system. In previous work,[26] we have shown that it is possible to calculate this accessible volume analytically. The analytical calculation is based on an extension of the work of Dodd and Theodorou,[30] which was able to evaluate the accessible volume for a sphere in an arbitrary configuration of fused spheres. In our case, we construct m hard spheres, i, off of each atom,[26] j, constituting the N_1 solvent and $N_2 - 1$ solute molecules and attribute a radius, d_{ij}, to each sphere. The total volume of the set of hard spheres generated in this way corresponds to the locus of points where insertion of the first atom of the N_2^{th} solute molecule as a hard-sphere molecule will result in an overlap. The hard-sphere diameters, d_i, attributed to each atom may have either the same value or a value depending on the atom type. The choice of optimal values follows the same criteria as that in SPD.[24−26]

To recapitulate, we choose $\int g(x,y)\,dx$ as $\int H_{\mathbf{q}_{N_1},\mathbf{q}_{N_2}}(\mathbf{r}_1^{(N_2)},d)\,d\mathbf{r}_1^{(N_2)}$, that is, the accessible volume for inserting the first atom of the N_2^{th} solute molecule in orientation/internal configuration $\mathbf{q}_{(N_2)}$ (specified by the last $3m$-3 elements of $\mathbf{q}_{N_2}$) within the solvent−solute configuration specified by $\mathbf{q}_{N_1}$ and the first $(N_2 - 1)m$ elements of $\mathbf{q}_{N_2}$. Equation 7 then becomes

$$R_Z = \frac{\int e^{-\beta PV} V^{N_1+N_2}\,dV \iint e^{-\beta U(\mathbf{q}_{N_1},\mathbf{q}_{N_2})}\,d\mathbf{q}_{N_1}\,d\mathbf{q}_{N_2}}{\int e^{-\beta PV} V^{N_1+N_2-1}\,dV \iiint \dfrac{\int H_{\mathbf{q}_{N_1},\mathbf{q}_{N_2}}(\mathbf{r}_1^{(N_2)},d)\,d\mathbf{r}_1^{(N_2)}}{\int H_{\mathbf{q}_{N_1},\mathbf{q}_{N_2}}(\mathbf{r}_1^{(N_2)},d)\,d\mathbf{r}_1^{(N_2)}} \times e^{-\beta U_2^{\text{intra}}(\mathbf{q}_{N_2})}\,d\mathbf{q}_{(N_2)}\,e^{-\beta U(\mathbf{q}_{N_1},\mathbf{q}_{N_2-1})}\,d\mathbf{q}_{N_1}\,d\mathbf{q}_{N_2-1}} =$$

$$\frac{\int e^{-\beta PV} V^{N_1+N_2}\,dV \iint e^{-\beta U(\mathbf{q}_{N_1},\mathbf{q}_{N_2})}\,d\mathbf{q}_{N_1}\,d\mathbf{q}_{N_2}}{\int e^{-\beta PV} V^{N_1+N_2-1}\,dV \iiiint \dfrac{1}{\int H_{\mathbf{q}_{N_1},\mathbf{q}_{N_2}}(\mathbf{r}_1^{(N_2)},d)\,d\mathbf{r}_1^{(N_2)}} \times H_{\mathbf{q}_{N_1},\mathbf{q}_{N_2}}(\mathbf{r}_1^{(N_2)},d)\,d\mathbf{r}_1^{(N_2)}\,e^{-\beta U_2^{\text{intra}}(\mathbf{q}_{N_2})}\,d\mathbf{q}_{(N_2)}\,e^{-\beta U(\mathbf{q}_{N_1},\mathbf{q}_{N_2-1})}\,d\mathbf{q}_{N_1}\,d\mathbf{q}_{N_2-1}} \tag{10}$$

Switching variables from $\mathbf{r}_1^{(N_2)}$ to $\mathbf{s}_1^{(N_2)}$ in the denominator

$$R_Z = \frac{\int e^{-\beta PV} V^{N_1+N_2}\,dV \iint e^{-\beta U(\mathbf{q}_{N_1},\mathbf{q}_{N_2})}\,d\mathbf{q}_{N_1}\,d\mathbf{q}_{N_2}}{\int e^{-\beta PV} V^{N_1+N_2}\,dV \iiiint \dfrac{1}{V\int H_{\mathbf{q}_{N_1},\mathbf{q}_{N_2}}(\mathbf{s}_1^{(N_2)},d/L)\,d\mathbf{s}_1^{(N_2)}} \times H_{\mathbf{q}_{N_1},\mathbf{q}_{N_2}}(\mathbf{s}_1^{(N_2)},d/L)\,d\mathbf{s}_1^{(N_2)}\,e^{-\beta U_2^{\text{intra}}(\mathbf{q}_{(N_2)})} \times d\mathbf{q}_{(N_2)}\,e^{-\beta U(\mathbf{q}_{N_1},\mathbf{q}_{N_2-1})}\,d\mathbf{q}_{N_1}\,d\mathbf{q}_{N_2-1}}$$

Recognizing that $d\mathbf{q}_{N_1}\,d\mathbf{q}_{N_2-1}\,\mathbf{d}s_1^{(N_2)}\,d\mathbf{q}_{(N_2)} = d\mathbf{q}_{N_1}\,d\mathbf{q}_{N_2}$, utilizing eq 5 for the energies, and invoking the equality $H_{\mathbf{q}_{N_1},\mathbf{q}_{N_2}}(\mathbf{s}_1^{(N_2)},d/L) = H_{\mathbf{q}_{N_1},\mathbf{q}_{N_2}}(\mathbf{r}_1^{(N_2)},d)$, we obtain

$$R_Z = \frac{\int e^{-\beta PV} V^{N_1+N_2}\,dV \iint e^{-\beta U(\mathbf{q}_{N_1},\mathbf{q}_{N_2})}\,d\mathbf{q}_{N_1}\,d\mathbf{q}_{N_2}}{\int e^{-\beta PV} V^{N_1+N_2}\,dV \int\int \dfrac{1}{V\int H_{\mathbf{q}_{N_1},\mathbf{q}_{N_2}}(\mathbf{s}_1^{(N_2)},d/L)\,d\mathbf{s}_1^{(N_2)}} \times H_{\mathbf{q}_{N_1},\mathbf{q}_{N_2}}(\mathbf{r}_1^{(N_2)},d)\,e^{+\beta U_{(N_2)}^{\text{inter}}(\mathbf{q}_{N_1},\mathbf{q}_{N_2})}\,e^{-\beta U(\mathbf{q}_{N_1},\mathbf{q}_{N_2})}\,d\mathbf{q}_{N_1}\,d\mathbf{q}_{N_2}} \tag{11}$$

From eq 11, it is clear that the inverse of R_Z can be expressed as an ensemble average in the N_1N_2PT ensemble

$$R_Z = \frac{1}{\left\langle \dfrac{1}{\int H_{\mathbf{q}_{N_1},\mathbf{q}_{N_2}}(\mathbf{s}_1^{(N_2)},d/L)\,d\mathbf{s}_1^{(N_2)}} \times H_{\mathbf{q}_{N_1},\mathbf{q}_{N_2}}(\mathbf{r}_1^{(N_2)},d)\dfrac{\exp\left(\beta U_{(N_2)}^{\text{inter}}(\mathbf{q}_{N_1},\mathbf{q}_{N_2})\right)}{V} \right\rangle} \tag{12}$$

Combining eqs 6, 7, and 12 we obtain the excess chemical potential as

$$\beta\mu_2^{\mathrm{ex}} = \ln\left[\left\langle\frac{1}{V}\right\rangle^{-1}\left\langle\frac{1}{\int H_{\mathbf{q}_{N_1},\mathbf{q}_{N_2}}(\mathbf{s}_1^{(N_2)}, d/L)\, d\mathbf{s}_1^{(N_2)}}\right.\right.$$
$$\left.\left. H_{\mathbf{q}_{N_1},\mathbf{q}_{N_2}}(\mathbf{r}_1^{(N_2)}, d)\frac{\exp\left(\beta U_{(N_2)}^{\mathrm{inter}}(\mathbf{q}_{N_1}, \mathbf{q}_{N_2})\right)}{V}\right\rangle\right] \quad (13)$$

By entirely analogous arguments, one can prove the validity of eq 13 in the canonical ensemble; in that case, all terms involving the volume are constant and cancel out, leading to a simpler expression.

We have used eq 13 to compute the excess chemical potential of CO_2 from our N_1N_2PT simulations of PS/CO_2 systems. In each configuration analyzed, a CO_2 molecule was picked at random. The equivalent hard solute molecule was constructed according to prescribed d values assigned to various atom types. (Please see below.) In the case of at least one overlap between any of the three spheres of the hard solute and the spheres of the atoms constituting the surrounding PS and remaining CO_2 molecules, a contribution of zero was entered in the averaging process, as required by the $H_{\mathbf{q}_{N_1},\mathbf{q}_{N_2}}(\mathbf{r}_1^{(N_2)},d)$, term on the right-hand side of eq 13. If no overlap was found, then we proceeded to calculate analytically[26,30] the accessible volume fraction $\int H_{\mathbf{q}_{N_1},\mathbf{q}_{N_2}}(\mathbf{s}_1^{(N_2)},d/L)\, d\mathbf{s}_1^{(N_2)}$ for the selected CO_2 molecule at fixed internal geometry and orientation within the current configuration of the PS matrix and remaining CO_2 molecules. This accessible volume fraction is guaranteed to be nonzero by the condition of no overlap at the initial position of the CO_2 molecule. Next, we computed the intermolecular potential energy $U_{(N_2)}^{\mathrm{inter}}(\mathbf{q}_{N_1},\mathbf{q}_{N_2})$ felt by the selected CO_2 molecule because of its interactions with the PS matrix and other CO_2 molecules; this is the energy we would obtain upon conversion of the selected molecule into a hard solute in the current configuration. Finally, we accumulated the term in the second bracket within the logarithm on the right-hand side of eq 13. This procedure was repeated with every CO_2 molecule in the analyzed configuration. Averaging was performed over all removals and all configurations, as indicated in eq 13. A simple flow diagram of DPD calculations is given in Scheme 1.

Given that $U_{(N_2)}^{\mathrm{inter}}(\mathbf{q}_{N_1},\mathbf{q}_{N_2})$ appears with a positive sign within the exponential on the right-hand side of eq 13, the reader may be tempted into thinking that μ_2^{ex} is mainly shaped by unfavorable, high-energy configurations of the solute molecule, which are not likely to be sampled in a canonical or isothermal−isobaric simulation. This is not true. The term $H_{\mathbf{q}_{N_1},\mathbf{q}_{N_2}}(\mathbf{r}_1^{(N_2)},d)$ that precedes the exponential clips such high-energy and overlaps

Scheme 1

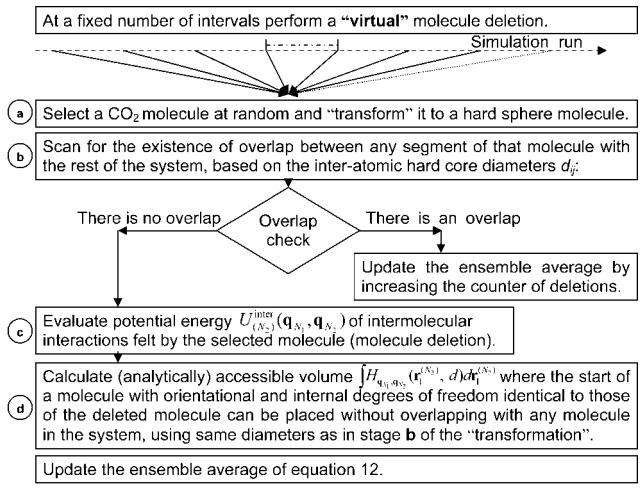

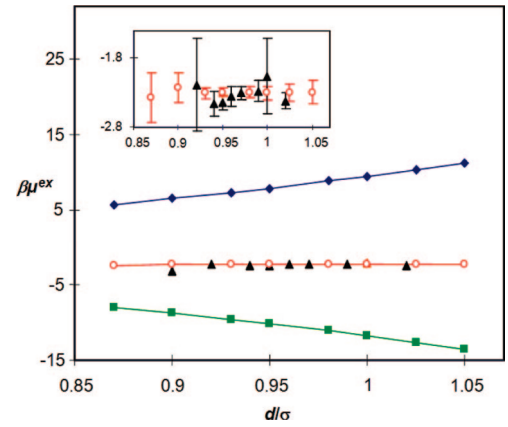

Figure 1. Test of the direct particle deletion (DPD) method for calculation of chemical potential. The excess chemical potential based on DPD (▲) and on the two-stage single particle deletion (SPD) scheme (○) is shown as a function of the hard-sphere diameter employed by the methods for a Lennard-Jones fluid at $T = 1$ and $\rho = 0.8$ (reduced units), as obtained in the course of canonical Monte Carlo simulation. The two constituent terms computed via SPD are also shown: free volume (♦) and energy (■). Statistical uncertainties, as obtained from postprocessing calculations with comparable requirements in computer time, are shown in the inset, where the scale of the ordinate has been expanded. Results are in perfect agreement[25] with Widom insertion (-2.30 ± 0.07) and with the analytical value from an accurate empirical equation of state (-2.27) for this system.

configurations so that modest and low-energy configurations of the solute, sampled readily in the course of a simulation, shape the ensemble average. As discussed below, the statistical efficiency of the method can be tuned by the selection of the hard-sphere diameters, d, and there is a relatively broad range of d for which good results are obtained.

As a test case for our method, we present in Figure 1 a comparison of DPD and SPD in the evaluation of the excess chemical potential in a pure LJ fluid at $T = 1$ and $\rho = 0.8$ (in reduced units). The hard core diameter, d, utilized in the two methods has been systematically varied. Results from both methods are in perfect agreement with the Widom insertion method (-2.30 ± 0.07) and with the analytical result from an accurate empirical equation of state for the LJ fluid (-2.27). The conditions and simulation details of this calculation are identical to those reported in ref 25. In Figure 1, we have also plotted the two contributions (from accessible volume and from the free energy of transforming the molecule into a hard sphere), as dictated by SPD.[25] The same agreement has been found under all conditions that we have investigated.

The SPD and DPD methods are very powerful for dense systems and large solute molecules in comparison with traditional Widom insertion. Apart from their efficiency, particle deletion schemes offer the unique ability of rigorously relating the solubility to the cost of creating a cavity. This has proved to be valuable in efforts to understand the molecular origin of the hydrophobic effect.[40] DPD offers comparable precision and accuracy to that of SPD (which has been shown to be superior to more traditional insertion-based methods[25,26]) and has the additional advantage of giving the result in one step by straightforward postprocessing of a canonical or isothermal−isobaric simulation of the solvent−solute system.

From Figure 1, one can see that, as is the case with SPD, the DPD method offers relative freedom in the choice of the hard core diameter (d or d/L in units reduced with the box length) for each of the spheres (atom types in the system). Lower limits on the d values employed can be set by requiring that, for any pair interaction between atom i of the N_2^{th} solute molecule and atom j in the system, $d_{ij} = (d_i + d_j)/2$ exceed the distance at which the pair distribution function $g(r)$ for that pair departs

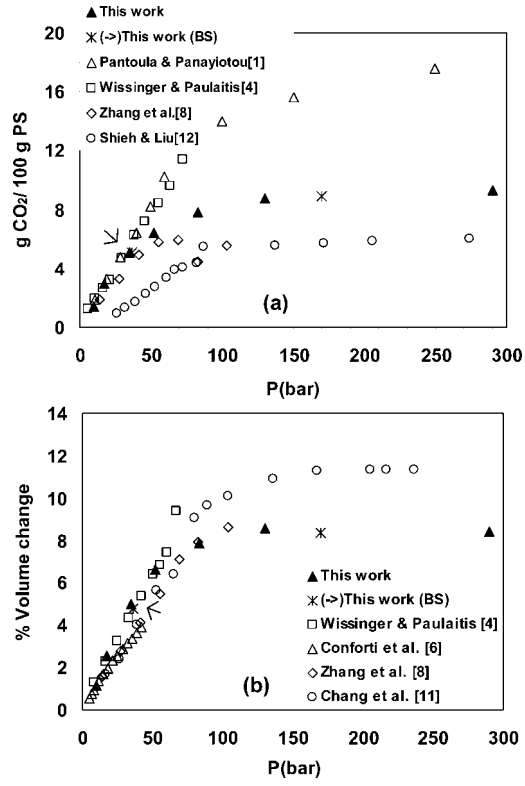

Figure 2. Comparison of simulation results and experimental data for (a) the sorption of CO_2 in PS and (b) the induced swelling at $T = 308$ K for pressures up to 300 bar. At this temperature, a bigger system (BS) was also simulated at two loadings (36.5 and 170 bar). Arrows have been drawn to facilitate locating the star symbols corresponding to the BS at the lower pressure. The results indicate that there are no system size effects.

from zero. The larger the diameter of the spheres, the higher the statistical error in the accessible volume calculation. As in the case of SPD, the optimal choice in terms of statistical error is made empirically in the vicinity of the LJ pair interaction diameters. More precisely, the PS matrix was viewed here as consisting of two types of hard-sphere sites: CH_2 (also used for CH_3) and CH, with diameters, d_i, 20% smaller than the LJ diameters of the aliphatic sites in the force field, that is, 3.457 and 3.322 Å, respectively. The diameters of the C and O centers of CO_2 were taken to be 10% larger than the corresponding LJ diameters, that is, 3.033 and 3.336 Å, respectively. This was found to be the best compromise between the fraction of deletions leading to nonzero contribution to the average and the speed of calculation. At the lowest CO_2 concentrations studied, where application of the Widom insertion method for the calculation of chemical potentials was practical, the chemical potential was also calculated by Widom insertion. Results from DPD and Widom insertion were found to be perfectly consistent.

Results

Sorption Isotherms and Swelling. In Figures 2−6 are shown the simulation results for the sorption of CO_2 in PS and the induced swelling as a function of pressure for $T = 35$, 50, 81, 100, and 132 °C, respectively, along with available experimental data for comparison. The large temperature and pressure range extends from the glassy state to the plastified polymer and the melt. The size of plotting symbols (▲,*) in Figures 2−6 is indicative of the standard deviation in our computer estimates of the fugacity and volume of the system. The fugacity (obtained by DPD) and the volume exhibited limited fluctuations around constant values throughout the production phase of the runs, indicating that our scheme for repartitioning CO_2 molecules was

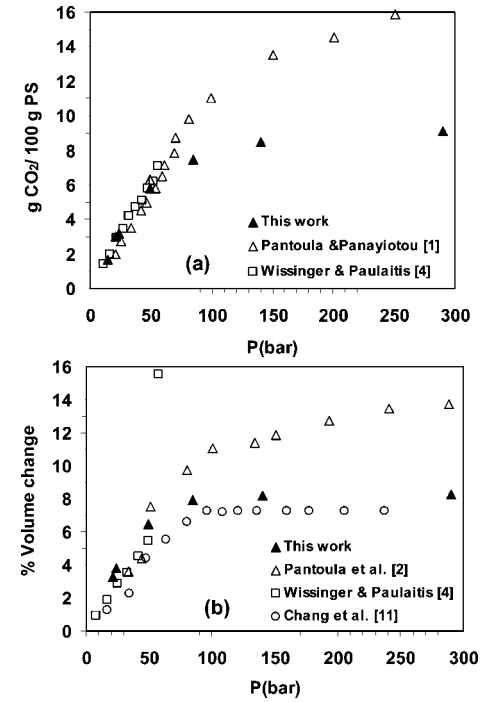

Figure 3. Comparison of simulation results and experimental data for (a) the sorption of CO_2 in PS and (b) the induced swelling at $T = 323$ K for pressures up to 300 bar.

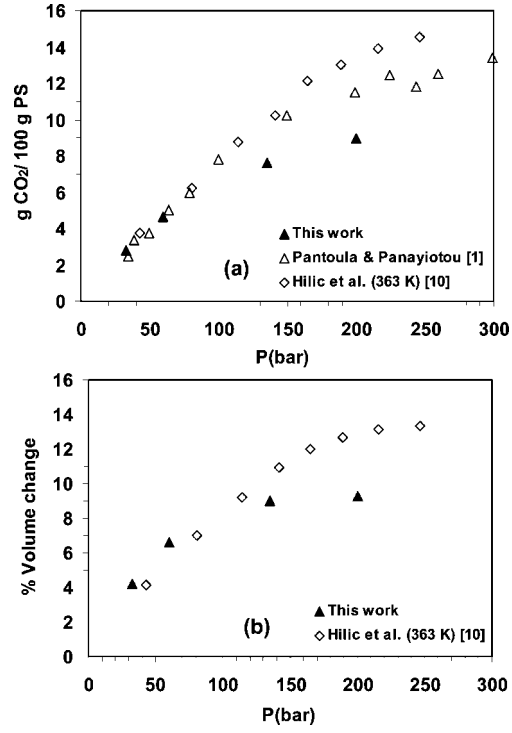

Figure 4. Comparison of simulation results and experimental data for (a) the sorption of CO_2 in PS and (b) the induced swelling at $T = 354$ K for pressures up to 300 bar.

effective in promoting equilibration. The comparison of predicted and experimental sorption and swelling behavior is very satisfactory at low T for pressures of <50 bar and at high T in the entire pressure range. At low T, the simulated polymer saturates at a lower concentration compared with the recent results of Panayiotou and collaborators.[1,2] The quality of the simulated glass (ultrafast quenching history of formation and its consequences on free volume distribution), given the long

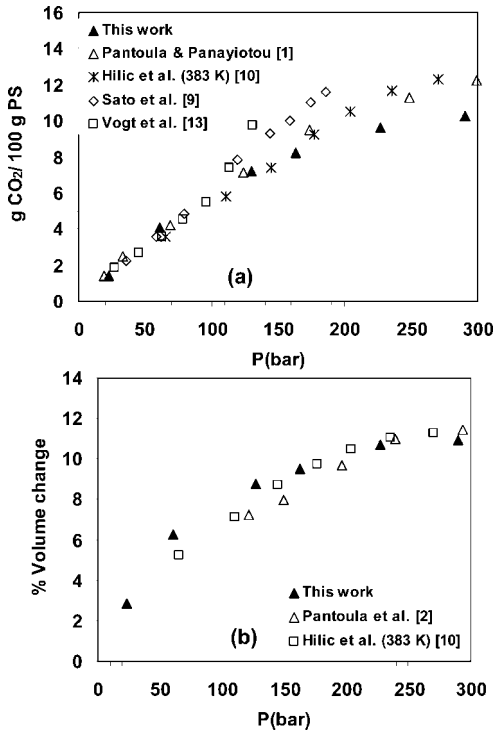

Figure 5. Comparison of simulation results and experimental data for (a) the sorption of CO_2 in PS and (b) the induced swelling at $T = 373$ K for pressures up to 300 bar.

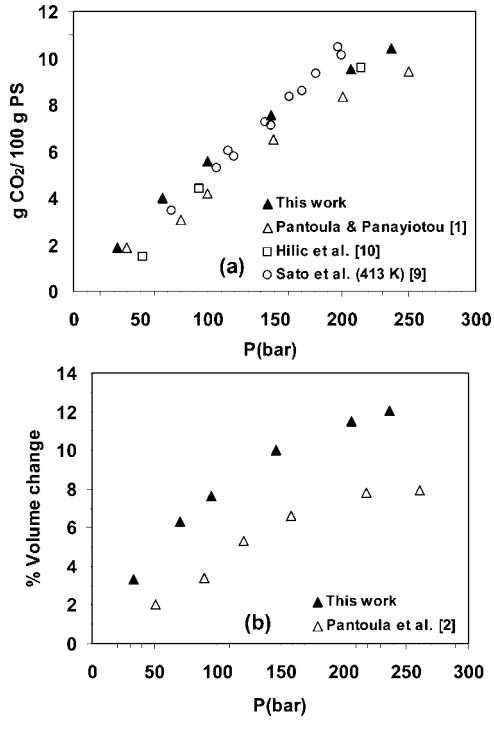

Figure 6. Comparison of simulation results and experimental data for (a) the sorption of CO_2 in PS and (b) the induced swelling at $T = 405$ K for pressures up to 300 bar.

relaxation times of the polymer (see below), is the most probable origin of these discrepancies. The experimental data themselves show a large scatter at low temperatures and high pressures. At the lowest temperature (308 K), the bigger system (BS), containing approximately twice the number of sorption sites, showed very similar trends to the base-case system, as seen in Figure 2. This comparison indicates that there are no system size effects on the predicted sorption and swelling characteristics.

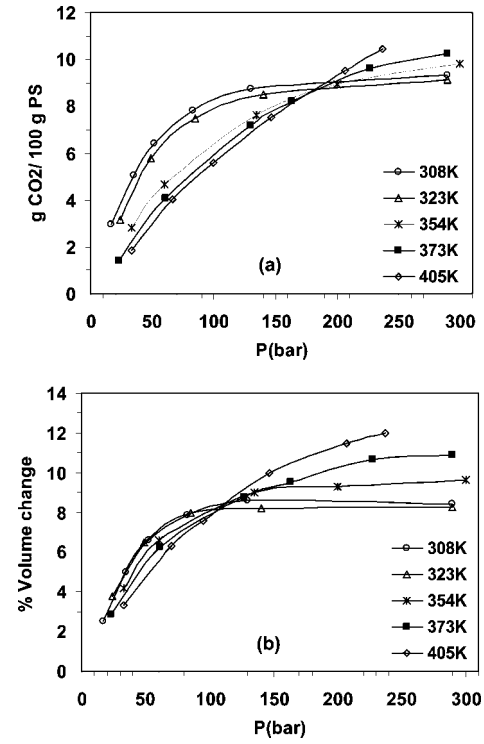

Figure 7. Simulation results for (a) the sorption of CO_2 in PS and (b) the induced polymer swelling at various temperatures for pressures up to 300 bar. Lines have been drawn through the isothermal points by cubic spline interpolation to facilitate inspection of the trends.

Figure 7 depicts all predicted simulation isotherms and swelling curves to facilitate the inspection of the trends shown by the simulation results and a comparison of them at the various temperatures and pressures. It is seen that for low pressures (<100 bar) the trend in both the uptake of solute and the polymer swelling is to decrease with increasing temperature. This is a common trend in sorption of gases in polymers, although larger differences are observed experimentally between different temperatures.[1,2] Another feature that is captured well by our simulation results is the increasing linearity in the sorption curves at high temperatures, where the polymer is in the melt state. At high pressures, a leveling off is observed for both sorption and swelling at all temperatures. This behavior is more noticeable at low T (32 and 50 °C). The polymer seems to be saturated with solute. At higher temperatures and for high pressures, a crossing of the simulation curves is observed; that is, at higher T, the polymer can swell more and can accommodate more solute. This behavior can probably be explained in terms of the long, strongly temperature-dependent relaxation times of the matrix, as will be discussed later in connection with Figure 9.

The partial molar volume (PMV) and the partial molar enthalpy of CO_2 in PS can be derived from the sorption isotherms. The PMV can be obtained as the slope of the swelling versus concentration curve.[42] It was found that for all temperatures the PMV decreased with pressure until it reached a plateau value above 100 bar. The average value of this plateau was 18 and 38 cm^3/mol for 323 and 373 K, respectively (compared with 24 and 45 cm^3/mol calculated from Pantoula and Panayiotou's results under the same conditions[1]). Fleming and Koros[43] reported a PMV value for CO_2 in a silicone elastomer for a pressure range 0−5 MPa equal to 46.2 cm^3/mol. Briscoe and Zakaria[44] observed that, with increasing pressure above 5 MPa, the PMV of CO_2 in the elastomer drops to a value of ca. 30 cm^3/mol.

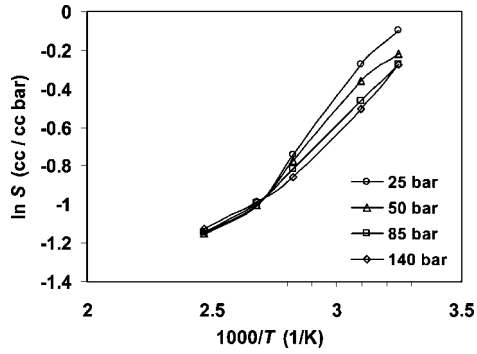

Figure 8. Temperature dependence of the solubility coefficient S (C/f) for various pressures. The slope of the curves provides an estimate of the partial molar enthalpy of the solute.

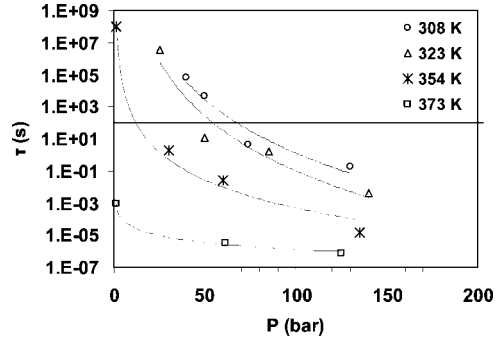

Figure 9. Calculated average relaxation times of the pendant CH(al)−C(ar) bond in PS as a function of pressure for the CO_2/PS systems at various temperature. The lines are best fits of the points. The drawn line at 100s indicates the glass transition.

In Figure 8 is shown the temperature dependence of the solubility coefficient S at constant pressure. S is defined as the ratio of the concentration, C (cm^3 (STP)/cm^3 pol), and the fugacity, f, of CO_2 at constant T and P. For constant P, S decreases with temperature, indicating lower solubility at high T. At low T, solubility decreases with increasing pressure. At high T, however, the curves for different pressures almost coincide. The partial molar enthalpy of sorption of CO_2 in PS, $\Delta\bar{H}_s$, can be calculated for each pressure as the slope of the curves in Figure 8. It was found that $\Delta\bar{H}_s$ ranged from −2.9 at low pressures to −2.2 kcal/mol at high pressures. From Pantoula and Panayiotou's results,[1] we calculated an average value of −4 kcal/mol for all pressures. The lower absolute values from the simulations are probably due to the weaker solute−matrix interactions (smaller ΔH_{mix}) caused by the charge-free molecular model invoked for PS. Costello and Koros[45] found that the $\Delta\bar{H}_s$ of CO_2 in glassy PC is −5.3 kcal/mol at 5 atm.

Dynamical Properties. The average segmental relaxation times for the pendant CH(al)−C(ar) bond of PS are depicted in Figure 9 as a function of pressure for T = 35, 50, 81, and 100 °C. They have been calculated by fitting the second-order correlation function $P_2(t)$ to a Kohlrausch−Williams−Watts (KWW) equation. The $P_2(t)$ autocorrelation function is defined as

$$P_2(t) = \frac{1}{2}\{3\langle[\mathbf{u}_{CH-C}(t)\cdot\mathbf{u}_{CH-C}(0)]^2\rangle - 1\} \qquad (14)$$

where $\mathbf{u}_{CH-C}(t)$ is the unit vector along the CH(al)−C(ar) bond of PS at time t. The $P_2(t)$ were accumulated over stretches of the MD trajectories that were free of exchanges of CO_2 molecules between cavities because exchanges were found to accelerate the polymer matrix dynamics artificially. The decay of $P_2(t)$ with time can be well described by a KWW equation

$$P_{KWW}(t) = \exp[-(t/\tau)^{\beta}] \qquad (15)$$

where τ is a characteristic time and β is the stretching exponent. The correlation times for the CH(al)−C(ar) bond of PS were estimated to be

$$\tau_c = \int_0^{\infty} P_2(t)\,dt \rightarrow \tau_c = \tau\frac{\Gamma\left(\frac{1}{\beta}\right)}{\beta} \qquad (16)$$

Values of β from the fit ranged from 0.1 to 0.13 in the glassy state and from 0.15 to 0.5 above the glass transition up to the melt. A line drawn at 100 s indicates the estimated CO_2 pressure, P_g, at which sorption-induced devitrification of the polymer occurs at each temperature. Long relaxation times are calculated for the low T systems, even within the plasticized regime at high pressures. Correlation times may differ by as much as 6 orders of magnitude between the lowest and highest temperatures studied in the high P (plasticized) regime.

The glass-transition pressures (P_g) estimated from the simulation as described above for each temperature are shown in Figure 10 along with experimental data. The comparison is quite satisfactory.

Free Volume Analysis. Gas sorption in glassy polymers, as envisioned by the well-known dual-mode model,[46] is due to sorption within large pockets of excess free volume present in the glass, described by the Langmuir mode, and liquid-like dissolution in small interstices between chains, described by Henry's law mode. To investigate the relationship between the observed sorption behavior and the free volume cavities in the systems, we have performed a geometric analysis of the free volume. The results presented in the following refer to the polymeric matrix devoid of the solute particles. The geometric analysis follows the approach of Greenfield and Theodorou.[29] Each polymer atom is assigned a hard-sphere radius. The volume accessible to the center of a hard-sphere solute (probe) with radius r_p is then found by augmenting the radii of all polymer atoms by r_p and calculating the remaining volume within each Delaunay tetrahedron formed by nearest-neighbor polymer atoms. Delaunay tetrahedra sharing a face that is not fully occupied at the r_p employed and would therefore permit the passage of a solute of radius $\leq r_p$ from one tetrahedron to another, are categorized as connected; they participate in the same cluster of accessible volume for all radii equal to or smaller than r_p. As the probe radius r_p is augmented, the clusters of accessible volume tend to become fewer and disjoint. In Figure 11 is depicted the average accessible fractional free volume (FFV) calculated over 30 configurations for the same CO_2 concentration (35 cm^3(STP)/cm^3 pol) at 308, 373, and 405 K as a function of the probe radius, r_p. At this concentration, the system at 308 K is in the glassy state, whereas at the other two temperatures, it is in the melt. As expected, the FFV decreases

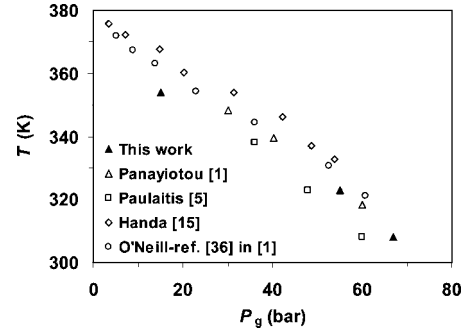

Figure 10. Comparison of simulation and experiments for the sorption-induced glass-transition pressures at temperatures below the T_g of pure PS.

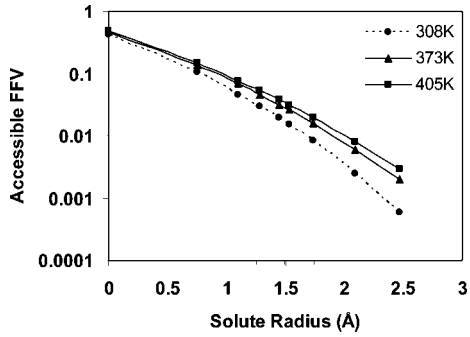

Figure 11. Accessible fractional free volume as a function of solute radius for a PS/CO_2 system of concentration 35 cm^3 (STP) CO_2/cm^3 pol at 308, 373, and 405 K. At the specific concentration, the system at 308 K is in the glassy state. Lines have been drawn through the points by cubic spline interpolation at each temperature.

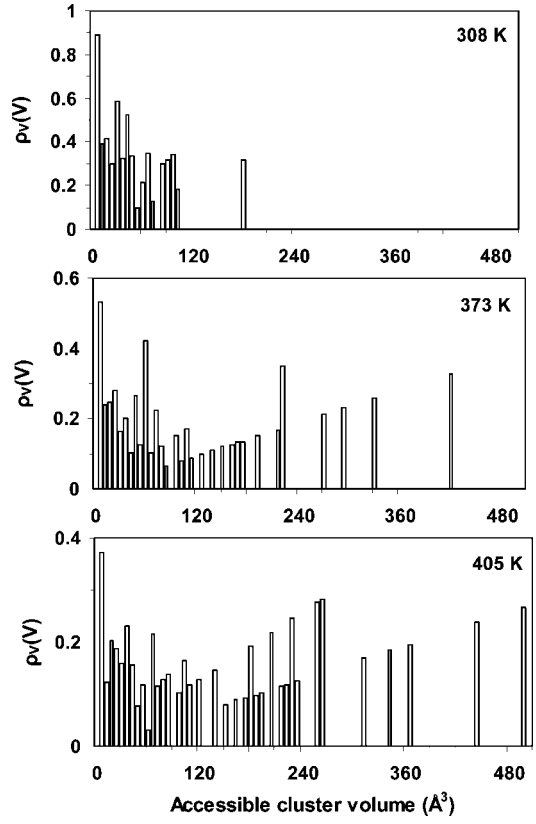

Figure 12. Volume-weighted distribution of free volume for a PS/CO_2 system of concentration 35 cm^3 (STP) CO_2/cm^3 pol at 308, 373, and 405 K for a solute radius equal to 2.1 Å. The solute molecules have been subtracted from the matrix for the free volume calculations.

with increasing probe radius. Another observation is that the FFV increases with the temperature because the matrix swells more at the higher temperatures. In Figure 12 is shown the average volume-weighted distribution of accessible cluster volume for a probe radius equal to 2.1 Å for the same system examined in Figure 11 at 308, 373, and 405 K. It is observed that clusters of higher accessible volume are found as the temperature increases, following the overall swelling of the matrix. From Figures 11 and 12 we conclude that our systems exhibit a rather continuous size distribution of the pockets of free volume encountered in them. We do not see evidence of trapped excess free volume[43] in the glass, as generated in our calculations by rapid cooling from the melt.

Conclusions

A strategy allowing the computation of sorption isotherms up to high penetrant fugacities in glassy matrices has been designed. We loaded glassy matrices of PS obtained from coarse-graining, equilibration, and reverse-mapping[23] with CO_2 at various compositions by mapping the accessible free volume. The new strategy permits an equilibrium repartitioning of CO_2 in the thermally fluctuating polymer matrix, via CO_2 displacements between accessible cavities, performed according to a microscopically reversible scheme. The scheme is coupled to an efficient methodology for the calculation of the penetrant fugacity, that is, the DPD method, a generalization of the SPD method.[25] The sorption isotherms of CO_2 in atactic PS and the induced polymer swelling have been calculated in the temperature range from 308 to 405 K and for pressures up to 300 bar. The large temperature and pressure range extend from the glassy state to the plastified polymer and the melt. The results compare favorably with available experimental data. Larger deviations are observed at low temperatures and high pressures, where the experimental data themselves show a large scatter. It is seen that for low pressures (below 100 bar) the trend in both the uptake of solute and the polymer swelling is to decrease with increasing temperature at fixed pressure. Swelling increases with increasing temperature at constant CO_2 concentration. Another feature is the increase in linearity in the sorption curves at high temperatures, where the polymer is in the melt state. At high pressures, a leveling-off is observed for both sorption and swelling at all T. This behavior is more noticeable at low T (32 and 50 °C). The polymer seems to be saturated with solute. At higher temperatures and for high pressures, a crossover of curves is observed (Figure 7); that is, at higher T values the polymer can swell more and accommodate more solute. This behavior can probably be explained in terms of the long relaxation times of the matrix at low temperatures, even in the plasticized regime.

Derivative properties, such as the PMV and the partial molar enthalpy of CO_2, have been calculated in good agreement with experimental findings.

Time autocorrelation functions have been computed for the pendant CH(al)−C(ar) bond of PS at each temperature as a function of pressure. Predicted correlation times (τ) were used to locate the glass-transition pressure (P_g) at each temperature by setting $\tau = 100$s, and the results compare well to experimental data. Correlation times were found to differ by as much as 6 orders of magnitude between the lowest and highest temperatures studied in the plasticized regime.

The analysis of the free volume showed that our systems exhibit a rather continuous size distribution of free volume cavities. We do not see evidence of trapped excess free volume in the glass, and higher free volumes are found, as expected, from the larger degree of swelling as temperature increases at fixed CO_2 concentration.

Acknowledgment. This work was supported by the European Commission through an NMP STREP project, contract NMP3-CT-2005-013644 (MULTIMATDESIGN). Support to GCB from the Senate Committee on Basic Research of the National Technical University of Athens in the form of a PEVE 2006 "Karathéodory" program is gratefully acknowledged.

Supporting Information Available: Animation illustrating cavities of accessible volume within the polymer and scheme for repartitioning CO_2 molecules among these cavities. This material is available free of charge via the Internet at http://pubs.acs.org.

References and Notes

(1) Pantoula, M.; Panayiotou, C. *J. Supercrit. Fluids* **2006**, *37*, 254.

(2) Pantoula, M.; von Schnitzler, J.; Eggers, R.; Panayiotou, C. *J. Supercrit. Fluids* **2007**, *39*, 426.
(3) Panayiotou, C.; Pantoula, M.; Stefanis, E.; Tsivintzelis, I. *Ind. Eng. Chem. Res.* **2004**, *43*, 6592.
(4) Wissinger, R. G.; Paulaitis, M. E. *J. Polym. Sci., Part B: Polym. Phys.* **1987**, *25*, 2497.
(5) Wissinger, R. G.; Paulaitis, M. E. *Ind. Eng. Chem. Res.* **1991**, *30*, 842.
(6) Conforti, R. M.; Barbari, T. A.; de Fernandes, P. M. E. *Macromolecules* **1996**, *29*, 6629.
(7) Aubert, J. H. *J. Supercrit. Fluids* **1998**, *11*, 163.
(8) Zhang, Y.; Gangwani, K. K.; Lemert, R. M. *J. Supercrit. Fluids* **1997**, *11*, 115.
(9) Sato, Y.; Yurugi, M.; Fujiwara, K.; Takishima, S.; Masuoka, H. *Fluid Phase Equilib.* **1996**, *125*, 129.
(10) Hilic, S.; Boyer, S. A. E.; Pádua, A. A. H.; Grolier, J.-P. E. *J. Polym. Sci., Part B: Polym. Phys.* **2001**, *39*, 2063.
(11) Chang, S.-H.; Park, S.-C.; Shim, J.-J. *J. Supercrit. Fluids* **1998**, *13*, 113.
(12) Shieh, Y.-T.; Liu, K.-H. *J. Supercrit. Fluids* **2003**, *25*, 261.
(13) Vogt, B. D.; RamachandraRao, V. S.; Gupta, R. R.; Lavery, K. A.; Francis, T. J.; Russell, T. P.; Watkins, J. *Macromolecules* **2003**, *36*, 4029.
(14) Toi, K.; Paul, D. R. *Macromolecules* **1982**, *15*, 1104.
(15) Zhang, Z.; Handa, Y. P. *J. Polym. Sci., Part B: Polym. Phys.* **1998**, *36*, 977.
(16) Alessi, P.; Cortesi, A.; Kikic, I.; Vecchione, F. *J. Appl. Polym. Sci.* **2003**, *88*, 2189.
(17) Van der Vegt, N. F. A.; Briels, W. J.; Wessling, M.; Strathmann, H. *J. Chem. Phys.* **1999**, *110*, 11061.
(18) Gusev, A. A.; Suter, U. W. *Phys. Rev. A* **1991**, *43*, 6488.
(19) Cuthbert, T. R.; Wagner, N. J.; Paulaitis, M. E. *Macromolecules* **1997**, *30*, 3058.
(20) Fukuda, M. *J. Chem. Phys.* **2000**, *112*, 478.
(21) Deitrick, G. L.; Scriven, L. E.; Davis, H. T. *J. Chem. Phys.* **1989**, *90*, 2370.
(22) Boulougouris, G. C.; Theodorou, D. N. *J. Chem. Phys.* **2007**, *127*, 084903.
(23) Spyriouni, T.; Tzoumanekas, C.; Theodorou, D.; Müller-Plathe, F.; Milano, G. *Macromolecules* **2007**, *40*, 3876.
(24) Boulougouris, G. C. Ph.D. Thesis, National Technical University of Athens, **2001**,
(25) (a) Boulougouris, G. C.; Economou, I. G.; Theodorou, D. N. *Mol. Phys.* **1999**, *96*, 905.
(26) Boulougouris, G. C.; Economou, I. G.; Theodorou, D. N. *J. Chem. Phys.* **2001**, *115*, 8231.
(27) Harris, J. G.; Yung, K. H. *J. Phys. Chem.* **1995**, *99*, 12021.
(28) Plimpton, S. *J. Comput. Phys.* **1995**, *1*, 117.
(29) Greenfield, M. L.; Theodorou, D. N. *Macromolecules* **1993**, *26*, 5461.
(30) Dodd, L. R.; Theodorou, D. N. *Mol. Phys.* **1991**, *72*, 1313.
(31) Chapman, W. G.; Gubbins, K. E.; Jackson, G.; Radosz, M. *Ind. Eng. Chem. Res.* **1990**, *29*, 1709.
(32) Widom, B. *J. Chem. Phys.* **1963**, *39*, 2802.
(33) Boulougouris, G. C.; Frenkel, D. *J. Chem. Theory Comput.* **2005**, *1*, 389.
(34) Frenkel, D.; Mooij, G. C. A. M.; Smit, B. *J. Phys.: Condens. Matter* **1992**, *4*, 3053.
(35) Swope, W. C.; Andersen, H. C. *J. Phys. Chem.* **1984**, *88*, 6548.
(36) Lyubartsev, A. P.; Martsinovskii, A. A.; Shavkunov, S. V.; Vorontsov-Velyaminov, P. N. *J. Chem. Phys.* **1992**, *96*, 1776.
(37) Van der Vegt, N. F. A.; Briels, W. J. *J. Chem. Phys.* **1998**, *109*, 7578.
(38) Theodorou, D. N. *J. Chem. Phys.* **2006**, *124*, 034109.
(39) Hess, B.; Peter, C.; Ozal, T.; van der Vegt, N. F. *Macromolecules* **2008**, *41*, 2283.
(40) Jarzynski, C. *Phys. Rev. Lett.* **1997**, *78*, 2690.
(41) Boulougouris, G. C.; Voutsas, E. C.; Economou, I. G.; Theodorou, D. N.; Tassios, D. P. *J. Phys. Chem. B* **2001**, *105*, 7792–7798.
(42) De Angelis, M. G.; Merkel, T. C.; Bondar, V. I.; Freeman, B. D.; Doghieri, F.; Sarti, G. C. *J. Polym. Sci., Part B: Polym. Phys.* **1999**, *37*, 3011.
(43) Fleming, G. K.; Koros, W. J. *Macromolecules* **1986**, *19*, 2285.
(44) Briscoe, B. J.; Zakaria, S. *J. Polym. Sci., Part B: Polym. Phys.* **1991**, *29*, 989.
(45) Costello, L. M.; Koros, W. J. *Ind. Eng. Chem. Res.* **1992**, *31*, 2708.
(46) Barrer, R. M.; Barrie, J. A.; Slater, J. *J. Polym. Sci.* **1958**, *27*, 177.

MA8015294